Nanoparticle-mediated drug delivery to tumor vasculature suppresses metastasis

Eric A. Murphy*, Bharat K. Majeti*, Leo A. Barnes, Milan Makale, Sara M. Weis, Kimberly Lutu-Fuga, Wolfgang Wrasidlo, and David A. Cheresh†

Department of Pathology, Moores Cancer Center, University of California at San Diego, 3855 Health Sciences Drive, La Jolla, CA 92093

Communicated by Dennis A. Carson, University of California at San Diego School of Medicine, La Jolla, CA, April 17, 2008 (received for review March 7, 2008)

Integrin $\alpha v\beta 3$ is found on a subset of tumor blood vessels where it is associated with angiogenesis and malignant tumor growth. We designed an $\alpha v\beta 3$-targeted nanoparticle (NP) encapsulating the cytotoxic drug doxorubicin (Dox) for targeted drug delivery to the $\alpha v\beta 3$-expressing tumor vasculature. We observed real-time targeting of this NP to tumor vessels and noted selective apoptosis in regions of the $\alpha v\beta 3$-expressing tumor vasculature. In clinically relevant pancreatic and renal cell orthotopic models of spontaneous metastasis, targeted delivery of Dox produced an antimetastatic effect. In fact, $\alpha v\beta 3$-mediated delivery of this drug to the tumor vasculature resulted in a 15-fold increase in antimetastatic activity without producing drug-associated weight loss as observed with systemic administration of the free drug. These findings reveal that NP-based delivery of cytotoxic drugs to the $\alpha v\beta 3$-positive tumor vasculature represents an approach for treating metastatic disease.

antiangiogenic | intravital microscopy | pancreatic cancer | renal cell carcinoma | liposome

Angiogenesis contributes to tumor malignancy and is linked to a wide variety of inflammatory and ischemic diseases. Integrin $\alpha v\beta 3$, an internalization receptor for a number of viruses (1, 2), was shown to be preferentially expressed on the angiogenic endothelium in malignant or diseased tissues (3, 4). These characteristics of integrin $\alpha v\beta 3$ make it an attractive targeting molecule for molecular imaging and delivery of therapeutics for cancer. Previous studies have shown that $\alpha v\beta 3$-targeted nanoparticles (NPs) coupled to contrast agents can readily image the tumor vasculature revealing "hot spots" of angiogenesis within the tumor (5, 6). Therapeutic studies using the αv integrin-targeting peptide, RGD-4C, demonstrated that this peptide effectively targeted doxorubicin (Dox) to the tumor neovasculature and enhanced efficacy in human breast cancer xenografts in mice (7). In another study, an $\alpha v\beta 3$-targeted NP delivering a suicide gene to angiogenic blood vessels was capable of producing an anticancer response (8). Although integrin $\alpha v\beta 3$ is a marker of angiogenic endothelium, histological analysis of breast cancer biopsy tissue revealed that $\alpha v\beta 3$ was a primary marker of blood vessels within the most malignant tumors (4). In fact, a strong correlation was established between the percent of $\alpha v\beta 3$-positive vessels within the tumor and disease progression (9).

Here, we report the design and characterization of an $\alpha v\beta 3$-targeted NP capable of delivering various pharmacological agents to the $\alpha v\beta 3$-expressing tumor vasculature. Evidence is provided that an $\alpha v\beta 3$-targeted NP carrying the cytotoxic drug Dox is capable of controlling the metastatic behavior of pancreatic and renal cell cancer in mice. Importantly, targeted delivery of Dox to the tumor vasculature provided a 15-fold increase in the efficacy of the drug while producing few, if any, side effects.

Results

Design of NPs Targeted to Angiogenic Endothelium. A schematic representation of the targeted NP (RGD-NP) (Fig. 1*A*), which is composed of distearoylphosphatidylcholine (DSPC), cholesterol, dioleoylphosphatidylethanolamine (DOPE), distearoylphosphatidylethanolamine (DSPE)-mPEG2000, and DSPE-cyclic RGDfK. After dehydration/rehydration and sonication, the NPs were stepwise extruded down through a minimum pore size of 100 nm. Dynamic light scattering demonstrated that the NPs had a mean hydrodynamic diameter of 105 nm and a zeta potential close to neutrality [supporting information (SI) Table S1]. A 6-(((4,4-difluoro-5-(2-thienyl)-4-bora-3a,4a-diaza-s-indacene-3-yl)styryloxy)acetyl) aminohexanoic acid, succinimidyl ester (BODIPY) 630/650 fluorophore was conjugated to DOPE, and this fluorescent lipid was incorporated into the particle at low concentration for imaging both *in vitro* and *in vivo* targeting. To address the specificity of the NPs for integrin $\alpha v\beta 3$, we performed binding studies on human umbilical vein endothelial cells (HUVECs) that express high levels of this integrin (Fig. 1*B*). HUVECs were pretreated with a 20-fold molar excess of either cRGDfK (targeting peptide) or cRADfK (control peptide), and the RGD-NPs were subsequently incubated with the cells. RGD-NPs bound and internalized within 20 min in the presence of the cRADfK peptide as expected, whereas the soluble cRGDfK peptide completely inhibited the binding of the RGD-NPs (Fig. 1*B*).

***In Vivo* Targeting of the RGD-NPs.** After establishing targeting *in vitro*, the RGD-NPs were tested for targeting to the tumor vasculature. M21L-GFP mouse melanoma cells (integrin $\alpha v\beta 3$ negative) were implanted in dorsal skin-fold window chambers and allowed to grow and become vascularized for 7 days. We then injected RGD-NPs (targeted) or RAD-NPs (nontargeted) and imaged both the tumor (GFP) and NPs (BODIPY) by confocal microscopy. RGD-NPs targeted the newly forming tips of the tumor neovasculature associated with the tumor margin within 2 h and reached maximum binding ≈5 h after i.v. injection, whereas the corresponding RAD-NP did not accumulate in the tumor neovasculature at all time points examined (Fig. 1*C*).

RGD-Dox-NPs Are Antiangiogenic. To study the antiangiogenic effect of the targeted NP, mice containing s.c. Matrigel plugs loaded with basic fibroblast growth factor (bFGF) were i.v. injected with NPs containing Dox. Angiogenesis was measured after 7 days by labeling the vasculature with fluorescein-labeled *Griffonia Simplicifolia* lectin (10). It is important to note that this is a model of normal angiogenesis induced by a proangiogenic factor and not a model of tumor angiogenesis. Animals treated with RGD-Dox-NPs (1 mg/kg total Dox) demonstrated vascular

Author contributions: E.A.M., B.K.M., S.M.W., W.W., and D.A.C. designed research; E.A.M., B.K.M., L.A.B., M.M., and K.L.-F. performed research; E.A.M., B.K.M., S.M.W., and D.A.C. analyzed data; and E.A.M., B.K.M., and D.A.C. wrote the paper.

The authors declare no conflict of interest.

*E.A.M. and B.K.M. contributed equally to this work.

†To whom correspondence should be addressed. E-mail: dcheresh@ucsd.edu.

This article contains supporting information online at www.pnas.org/cgi/content/full/0803728105/DCSupplemental.

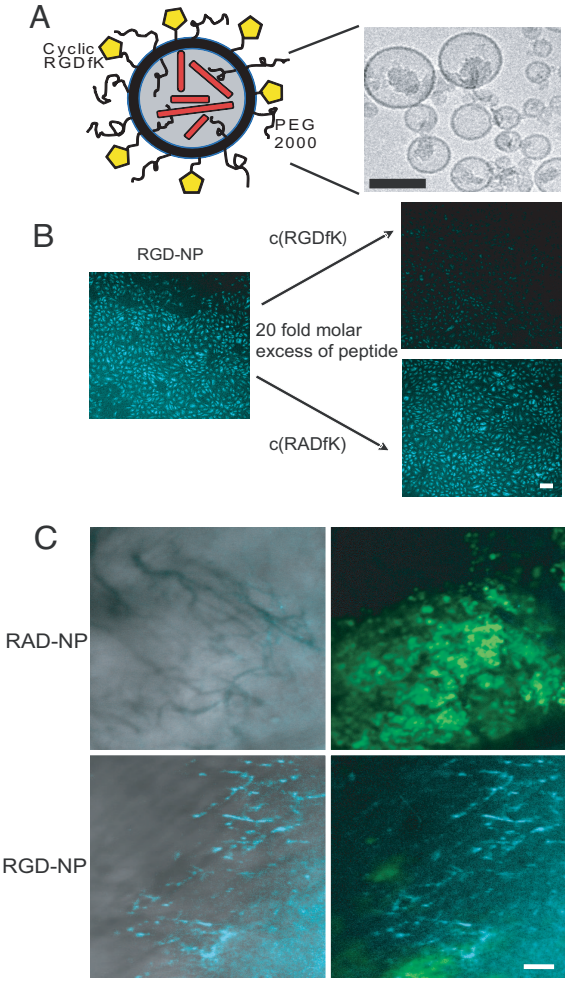

Fig. 1. *In vitro* and *in vivo* $\alpha v\beta 3$ targeting of RGD-NP. (*A*) Schematic representation and transmission EM of Dox-loaded RGD-NP. (*B*) Competition assay for *in vitro* $\alpha v\beta 3$ targeting of RGD-NP in endothelial cells. HUVECs were pretreated for 5 min with a 20-fold molar excess of either cRGDfK or cRADfK to test for inhibition of NP binding. Subsequently, the cells were incubated with the RGD-NPs for 20 min, and binding was studied by scanning confocal microscopy for the BODIPY 630/650 dye. (*C*) *In vivo* integrin $\alpha v\beta 3$ targeting of RGD-NPs within the tumor neovasculature was studied by intravital microscopy with the dorsal skin-fold window chamber. M21L melanomas ($\alpha v\beta 3$ negative) were allowed to vascularize for 7 days, and mice were i.v.-injected with 200 nmol of either RGD-NP or RAD-NP containing BODIPY 630/650. NPs were imaged by confocal scanning microscopy at 5-h postinjection. GFP-labeled M21L melanomas are shown in green, and NPs are in blue. (Scale bars: *A*, 100 nm; *B* and *C*, 100 μm.)

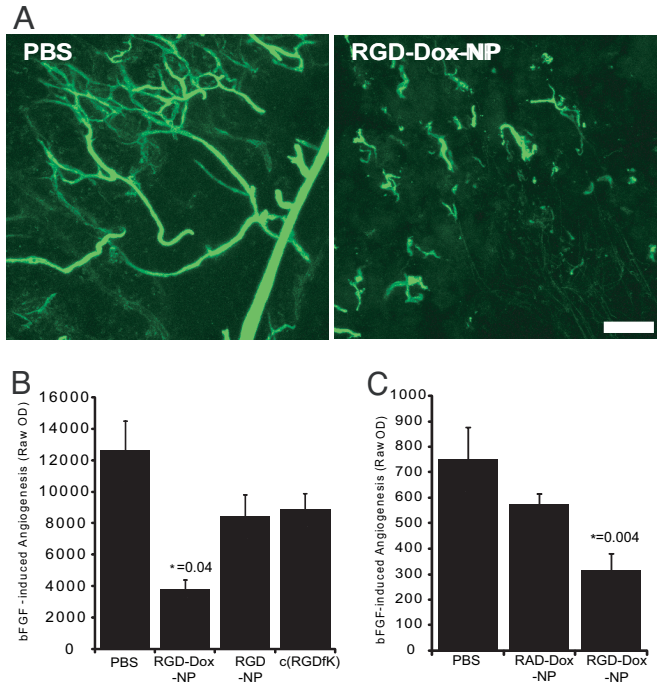

Fig. 2. Vascular disruption in the mouse Matrigel model with $\alpha v\beta 3$-targeted RGD-Dox-NP. Mice were injected s.c. on the flank with Matrigel containing 400 ng of human recombinant bFGF. NPs containing 1 mg/kg of Dox were i.v.-injected on days 1, 3, and 5. (*A*) After the treatment, mice were i.v.-injected with fluorescein-labeled *G. simplicifolia* lectin and the plugs were removed and imaged by scanning confocal microscopy. (*B* and *C*) To quantify angiogenesis, the matrigel plugs were removed and the fluorescent-lectin content was quantified with a fluorimeter. *, $P < 0.05$ for RGD-Dox-NP vs. PBS. (Scale bar: 100 μm.)

pruning when compared with the normal vascular structure and branching of animals treated with PBS (Fig. 2*A*) and inhibited angiogenesis by ≈70% (Fig. 2*B*). Although the cyclic RGDfK peptide has been previously shown to be an integrin $\alpha v\beta 3$ antagonist (11, 12), minimal response was observed when testing RGD-NP without Dox or cyclic peptide alone (Fig. 2*B*). Also, RAD-Dox-NPs demonstrated only a marginal reduction (24%) in neovascularization relative to control animals (Fig. 2*C*). These findings reveal that integrin $\alpha v\beta 3$ targeting of Dox containing NPs produces a strong antiangiogenic effect.

Comparison of RGD-Dox-NP Efficacy on Primary vs. Metastatic Sites in Pancreatic Carcinoma. We next evaluated the targeting and efficacy of the RGD-Dox-NPs in a syngeneic murine orthotopic tumor model of pancreatic carcinoma. R40P murine pancreatic cancer cells derived from a spontaneous murine pancreatic tumor (13) were injected into the tail of the pancreas. After 11 days of tumor growth, we injected fluorescent RGD-NPs i.v. and observed accumulation of the RGD-NPs in the pancreatic tumor vasculature but not in the vasculature of the adjacent normal pancreatic tissue (Fig. 3*A*). Additionally, tissues that manifest a filtration function exhibit detectable concentrations of NPs, albeit at significantly lower fluorescence intensities than the tumor tissue. Specifically, we observed minimal accumulation of the RGD-NPs in the kidney, liver, and lung but found no accumulation in the brain, heart, or spleen (Fig. 3 *A* and *B*).

For efficacy studies, mice implanted with orthotopic pancreatic tumors were treated on days 5, 7, and 9, and the effects of the RGD-Dox-NPs were observed on day 11. The primary pancreatic tumors were sectioned and analyzed by immunohistochemistry. The serial sections of primary tumors treated with RGD-Dox-NPs were stained with hematoxylin and eosin and analyzed for total blood vessels, $\beta 3$-positive blood vessels, and apoptosis (TUNEL stain) (Fig. 3*C*). For tumors treated with RGD-Dox-NPs at 1 mg/kg (as in Fig. 3*D*), we observed apoptosis in angiogenic hot spots that corresponded to the $\beta 3$ positive blood vessels associated with the tumor margin (Fig. 3*C*). No apoptosis was observed in areas corresponding to $\beta 3$-negative vessels. Additionally, no apoptosis was observed in tumors treated with the RAD-Dox-NPs, even when $\beta 3$-expressing blood vessels were present (data not shown).

Orthotopically implanted R40P cells typically form metastatic lesions in the hepatic hilar lymph node, which is important because regional lymph node metastasis is an important predictor for survival of pancreatic adenocarcinoma patients (14, 15).

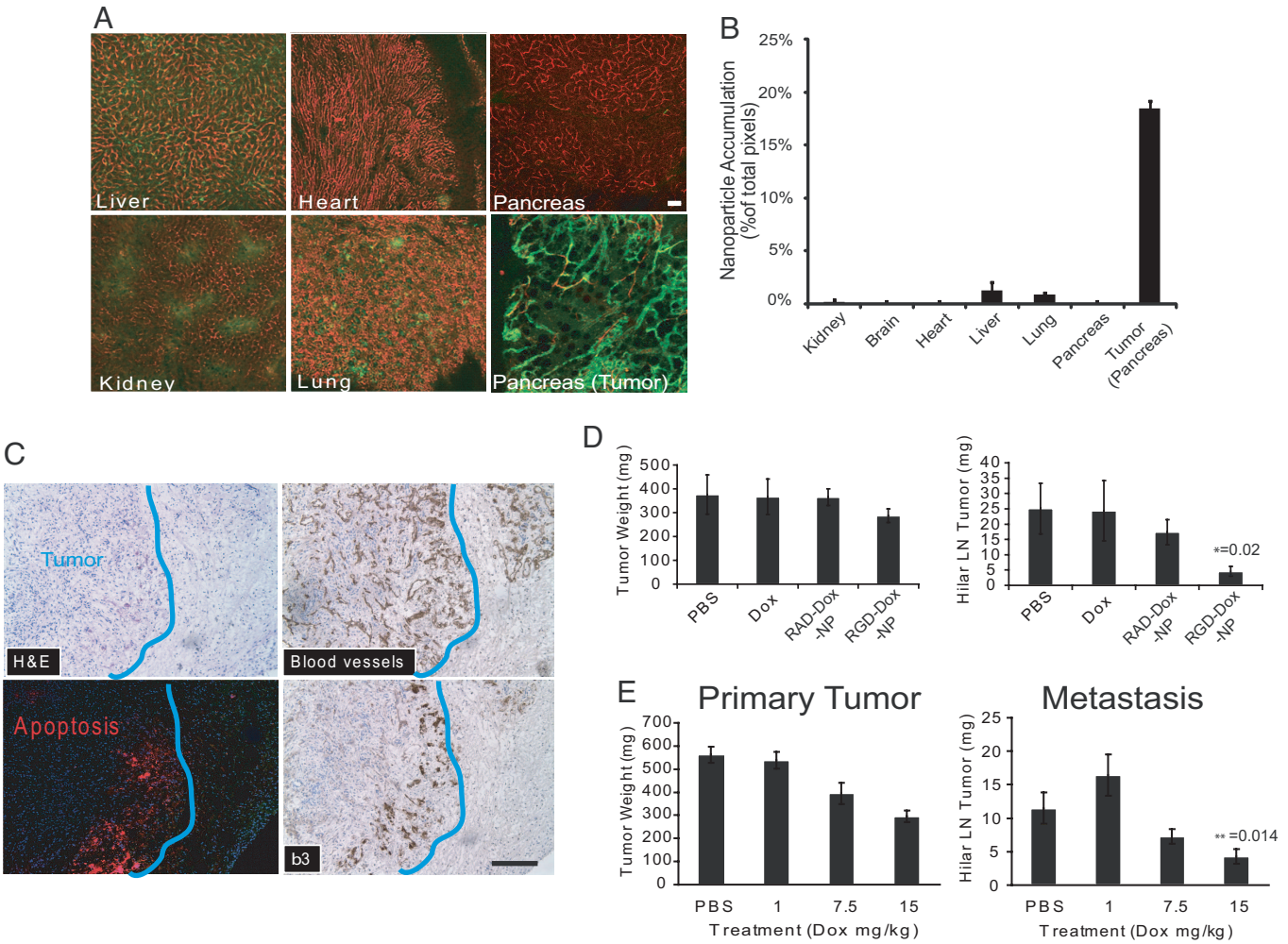

Fig. 3. Suppression of metastasis in an orthotopic model of pancreatic cancer. (*A*) R40P pancreatic carcinoma cells were injected into the tail of the pancreas in Tie-2 GFP mice and allowed to grow for 11 days. RGD-NPs labeled with BODIPY 630/650 were i.v.-injected, and the primary tumor, pancreas, liver, lung, kidney, and heart were imaged by confocal microscopy. Red represents rhodamine-labeled *G. simplicifolia* lectin for staining the endothelium, and green represents NP binding. (*B*) Quantitation of the fluorescent NPs in various tissues expressed as the percent of pixels from the confocal images. (*C*) Immunohistochemistry of serial sections from the tumors treated with the RGD-Dox-NPs demonstrates areas of apoptosis (TUNEL staining) that colocalize only with blood vessels that express the target (β3). (*D*) Integrin $\alpha v\beta 3$-targeted RGD-Dox-NPs prevent metastasis to the hepatic hilar lymph node. After surgical implantation of the cells, mice were treated on days 5, 7, and 9 with RGD-Dox-NP, RAD-Dox-NP, free Dox, or PBS (each with 1 mg/kg total Dox per dose). On day 11, the primary tumor and the hepatic hilar lymph node were resected and weighed. (*E*) Effect of free Dox at various concentrations (1, 7.5, and 15 mg/kg dosed on days 5, 7, and 9) on primary tumor growth and metastasis to the hepatic hilar lymph node. *, $P < 0.05$ for RGD-Dox-NP vs. PBS. **, $P < 0.05$ for 15 mg/kg free Dox vs. PBS. (Scale bars: *A* and *C*, 100 μm.)

To assess the effects of the RGD-Dox-NP on primary tumor growth and metastasis, tumor-bearing mice were injected with NPs on days 5, 7, and 9 after orthotopic tumor implantation. We then measured the size of the primary tumors and metastatic lesions on day 11. While the RGD-Dox-NPs containing 1 mg/kg of Dox produced a modest reduction of the primary tumor growth (23%), it significantly reduced metastasis to the hepatic hilar lymph node (82%) as compared with control animals (Fig. 3*D*). The untargeted particle, RAD-Dox-NPs containing 1 mg/kg Dox, had no significant effect on the primary tumor or the metastatic lesions (Fig. 3*D*). Importantly, 1 mg/kg of free Dox had no effect on either primary tumor growth or metastasis (Fig. 3*D*). Similarly, no antitumor effect was seen after separate administration of the empty RGD-NP together with 1 mg/kg free Dox (Fig. S1). To determine the concentration of free Dox that was necessary to duplicate the anticancer effects observed with the RGD-Dox-NPs we injected varying concentrations of free Dox and found that 15 mg/kg was required to achieve a similar reduction in metastasis as demonstrated with the RGD-NP containing 1 mg/kg Dox (Fig. 3 *D* and *E*). However, dosing animals with 15 mg/kg of free Dox caused severe weight loss (18% reduction in body weight), whereas the RGD-Dox-NP treatment at 1 mg/kg showed only a 0.8% decline in body weight (Fig. S2). Additionally, like the RGD-Dox-NP-treated animals, control animals did not gain or lose any weight during the experiment.

As an alternate treatment regimen, we increased the frequency of doses by treating animals on days 7, 8, and 9 after tumor implantation. In this case, we observed a more robust impact on the primary tumor (43% reduction vs. control) while maintaining a substantial antimetastatic effect (90% reduction vs. control) (Fig. S3). These studies suggest that targeting Dox to the tumor vasculature greatly affects metastasis.

Comparison of RGD-Dox-NP Efficacy on Primary vs. Metastatic Sites in Renal Cell Carcinoma. We further tested the NPs in an orthotopic model of renal cell carcinoma. In this model, human SN12C renal carcinoma cells expressing red fluorescent protein (RFP)

Table 1. Incidence of metastasis in the orthotopic renal cell carcinoma model

Metastatic site	RGD-DOX-NP	RAD-DOX-NP
Pancreas	5/8	6/8
Spleen	3/8	5/8
Diaphragm	1/8	4/8
Liver	1/8	4/8
Lungs	1/8	2/8
Gut	4/8	6/8
Primary	8/8	8/8

were injected into the left kidney of athymic nude mice. After 8 days, mice were dosed i.v. with either the RAD-Dox-NP or RGD-Dox-NP at 2 mg/kg total Dox every other day until the experiment was terminated on day 42. At that time point, control animals typically demonstrated widespread metastasis to the liver, spleen, diaphragm, and pancreas. However, treatment with the RGD-Dox-NP significantly reduced both the incidence of metastasis (Table 1) and the total metastatic burden (91%) (Fig. 4*A*). Images of the RFP-expressing metastatic lesions are shown for each of the metastatic sites in all animals (Fig. 4*B*). Metastasis was quantified by measuring the total pixels from each organ in both treatment groups. Similar to the pancreatic carcinoma results (Fig. 3*D*), there was only a modest reduction of primary tumor burden (35%) in the renal cell carcinoma model in animals treated with RGD-Dox-NPs compared with the RAD-Dox-NPs ($P = 0.27$) (Fig. 4*A*). Nevertheless, during the course of the NP treatment, the mice gained weight normally and displayed no obvious side effects (data not shown).

Discussion

Nontargeted long circulating liposomes, e.g., Doxil, have been extensively used for delivering chemotherapeutic drugs to tumors via the enhanced permeability and retention mechanism (16). Although liposomal delivery of cytotoxic drugs can improve antitumor activity, targeted delivery of these particles represents a potential approach to further enhance efficacy and minimize toxicity. Recent studies have described the design of NPs that target the tumor endothelium to improve diagnosis via imaging (5, 6, 17) or deliver therapeutics to solid tumors (8, 18, 19). The majority of the therapeutic research has focused on using various forms of RGD peptides for targeting integrin $\alpha v\beta 3$, which is present on the tumor neovasculature (20).

Integrin $\alpha v\beta 3$ represents an ideal vascular targeting receptor because it is highly expressed on the angiogenic endothelium and expression of this receptor on tumor vessels correlates with disease progression (9). Additionally, this receptor is used by viruses for internalization into cells, making it an optimal targeting receptor for NP-mediated drug delivery (21). By displaying targeting ligands such as cyclic RGD peptides in a multivalent array on the surface of NPs, avidity for the target is greatly increased as the binding to integrins causes both lateral diffusion and clustering of multimeric complexes (22, 23). This increase in avidity leads to active targeting even in the presence of shear stress generated by the flowing blood at the surface of the endothelium. The combination of these properties make integrin $\alpha v\beta 3$ a particularly useful target for delivering chemotherapeutic molecules to the tumor endothelium.

In this study, we evaluated the impact of integrin $\alpha v\beta 3$-targeted NP drug delivery on primary tumor growth and spontaneous metastasis of two orthotopic cancer models. Although we observed a reproducible, but modest, effect on primary tumor growth, we noted a substantial impact on metastatic disease. This effect was not based on integrin $\alpha v\beta 3$ expression on the tumor cells because the tumor cells examined in this study do not

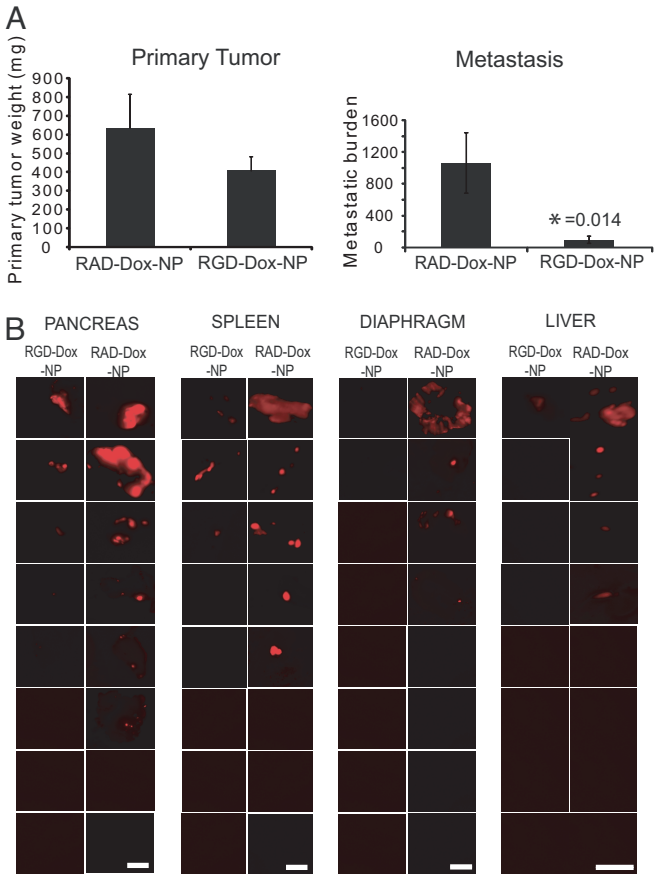

Fig. 4. RGD-Dox-NP reduces overall metastasis in an orthotopic renal cell carcinoma model. (*A*) Human SN12C-RFP cells were injected into the left kidney and primary tumors were established for 8 days. At that time, NPs containing 2 mg/kg Dox were dosed every other day from day 8 until day 42. At the endpoint, both kidneys were removed and the difference in weight was attributed to primary tumor burden. Additionally, the diaphragm, liver, pancreas, and spleen were resected and imaged for RFP-expressing metastatic lesions by using an OV-100 whole animal imaging system. The total pixels in each image were quantified by using ImageJ software and the average pixels of the metastatic lesions/animal are represented as the metastatic burden. *, $P < 0.05$ for RGD-Dox-NPs vs. RAD-Dox-NPs. (*B*) Images of the RFP fluorescence from the metastatic lesions present in the diaphragm, liver, pancreas, and spleen used for the quantification of the metastatic burden in *A* are presented for each animal. (Scale bars: 5 mm.)

express integrin $\alpha v\beta 3$. The modest effect on the primary tumor is perhaps not surprising, because treatment was initiated after the primary tumors had established a blood supply. Tumors with preestablished vasculature typically express integrin $\alpha v\beta 3$ on a subset of vessels associated with the tumor margin as we (Fig. 3*C*) and others have observed (4, 9). Because apoptosis is induced only in areas of the tumor colocalizing with $\beta 3$, only a fraction of the primary tumor (i.e., that near the margin) is expected to be impacted by the $\beta 3$-targeted NPs. Importantly, even though the hydrodynamic diameter of the untargeted RAD-Dox-NPs was 100–120 nm, no effect was observed on inhibition of primary tumor growth because of nonspecific accumulation in the tumor via the enhanced permeability and retention mechanism. Additionally, the untargeted RAD-Dox-NPs did not induce apoptosis in any area of the tumor (data not shown), confirming that targeting integrin $\alpha v\beta 3$ was necessary for localized tumor cell apoptosis.

Several hypotheses might help to explain the preferential effect of the RGD-Dox-NPs on the metastatic lesions in these

orthotopic tumor models. First, establishment of the blood supply might be much more critical at the newly forming metastatic sites relative to the established primary tumor, creating a differential sensitivity to the targeted treatment. Second, we demonstrate that RGD-Dox-NPs induce apoptosis in the β3-positive tumor vasculature (Fig. 3*C*), and this effect on the primary tumor could influence the invasive behavior of the tumor and its ability to metastasize. Third, in the tumor models examined here, to some degree primary tumor growth correlated with metastatic potential. For example, treatment of the pancreatic carcinomas with 7.5 or 15 mg/kg of free Dox reduced both the size of the primary tumor and the metastatic burden in the hepatic hilar lymph node (Fig. 3*E*). Further studies are necessary to elucidate the mechanism of the antimetastatic effect that might become important for other targeting strategies.

Using NP-mediated Dox delivery to the tumor vasculature, we were able to observe a 15-fold improvement in drug efficacy relative to animals treated with free drug (Fig. 3). Dox is dose-limited by cardiotoxicity (24), and lower doses greatly reduce the side effects of this chemotherapeutic agent. By targeting NPs to the tumor neovasculature, we observed an antitumor effect at 1 mg/kg of NP-encapsulated Dox with no appreciable weight loss, whereas 15 mg/kg of free Dox was required for similar efficacy, leading to an 18% decrease in body weight (Fig. S2). It will be interesting to use this approach with a number of the newer pharmacological agents designed to suppress tumor or vascular cell signal transduction (25). Although some of these agents are beginning to show promise in the clinic, targeted NP delivery would likely reduce the concentration needed for efficacy and minimize problems associated with pharmacokinetics and/or side effects.

Methods

Animal Studies. All animal procedures were conducted in accordance with all appropriate regulatory standards under protocol SO5018 and approved by the University of California San Diego Institutional Animal Care and Use Committee.

Cell Culture. M21L-GFP melanomas were maintained under standard culture conditions in DMEM supplemented with 10% FBS. R40P cells were isolated and cultured from a spontaneous pancreatic tumor in *Pdx1-Cre*,*LSL-KRas*^{G12D},*Ink4a/Arf*$^{lox/lox}$ mice after 7 weeks. Both the mice and tumor cell isolation procedure have been described (13). The R40P cells were maintained under standard culture conditions in RPMI medium 1640 supplemented with 10% FBS. SN12C-RFP cells were a gift from Robert Hoffman at AntiCancer, Inc. (San Diego). The SN12C-RFP renal carcinomas were grown in RPMI medium 1640 supplemented with 10% FBS and maintained under standard culture conditions. HUVECs were purchased from Lonza and maintained in EBM-2 with EGM-2 singlequots. HUVECs were propagated on plates coated with 10 μg/ml of collagen type I (Millipore), and all experiments were conducted at passage <6.

Synthesis of Peptide-Lipid Conjugates. The cyclic peptides, cRGDfK and cRADfK (f denotes D-phenylalanine), were synthesized by using standard Fmoc solid-phase chemistry as described (26). Peptides were purified by reverse-phase HPLC, and exact mass was confirmed by mass spectroscopy. For conjugation to lipid, the peptides were conjugated to a short linker, succinimidyl ester-$(PEO)_4$-maleimide (Pierce). DSPE was reacted with iminothiolane (Sigma–Aldrich) to produce a free thiol. The DSPE containing the free thiol group was reacted with the cRGDfK-$(PEO)_4$-maleimide or cRADfK-$(PEO)_4$-maleimide to produce the peptide-lipid conjugates, and those conjugates were recrystallized in methanol/diethyl ether 1:9 at 4°C overnight. The exact mass of the peptide-lipid conjugates was verified by mass spectroscopy.

NP Preparation. The particle formulation of cholesterol/DOPE/DSPC/DSPE-$(PEO)_4$-cRGDfK/DSPE-mPEG2000 (6:6:6:1:1 molar ratio) in chloroform was evaporated under argon gas, and the dried lipid film was hydrated in sterile 300 mM ammonium phosphate buffer (pH 7.4) in a total volume of 5 ml at a total lipid concentration of 3.32 mM for a minimum of 1 h. Liposomes were vortexed for 2–3 min to remove any adhering lipid film and sonicated in a bath sonicator (ULTRAsonik 28X) for 2–3 min at room temperature to produce multilamellar vesicles (MLVs). MLVs were then sonicated with a Ti-probe (Branson 450 sonifier) for 1–2 min to produce small unilamellar vesicles (SUVs) as indicated by the formation of a translucent solution. To reduce the size of the SUVs, stepwise extrusion was performed with the final step being extrusion through a polycarbonate filter with 100-nm pore size (Whatman). The buffer was exchanged with 20 mM Hepes, 150 mM NaCl, pH 7.4 by using gel-filtration chromatography (PD-10; GE Healthcare). Dox (Fluka) encapsulation was performed as described (27) with one slight variation in loading temperature. After addition of Dox to the NPs, the solution was heated at 55°C for 1h and then left overnight at room temperature before purification by PD-10 column, eluted with water. The amount of encapsulated Dox was quantified by adding 1.5% Triton X-100 to disrupt the NPs and comparing the absorbance at 476 nm on a spectrophotometer to a standard curve of free Dox.

***In Vitro* Competition Assay.** HUVECs were seeded and grown overnight in 48-well plates coated with 10 μg/ml collagen type I and blocked with 5% BSA. For competition, a 20-fold molar excess of either cRGDfK or cRADfK peptide was preincubated with the cells for 5 min in serum-free medium. NPs containing 1% of a BODIPY 630/650 (Invitrogen)-linked DOPE for fluorescence microscopy were added to the HUVECs for 20 min at 37°C. Cells were fixed and NP binding was visualized by confocal microscopy (Nikon C1si).

Dorsal Skin-Fold Window Chamber. Intravital microscopy of NP binding to the tumor neovasculature was monitored in the dorsal skin-fold window chamber as described (21, 22). Two days after surgical implantation of the window chamber, a concentrated (4 μl) suspension of 800,000 M21L-GFP melanoma cells was injected into the retractor muscle within the chamber. After 7 days and the appearance of tumor-associated angiogenesis, fluorescent RGD-NPs or RAD-NPs were injected i.v., and the animals were imaged 5 h postinjection by confocal microscopy (Nikon C1si).

***In Vivo* Angiogenesis.** The Matrigel assay was performed to assess *in vivo* angiogenesis (10). Briefly, mice were injected s.c. on the flank with 400 μl of growth factor-reduced Matrigel (BD Biosciences) containing either sterile saline or 400 ng of human recombinant bFGF (Millipore). After 7 days, mice were injected i.v. with 20 μg fluorescein-labeled *G. simplicifolia* lectin that binds selectively to mouse endothelial cells (GSL I–BSL I; Vector Labs). The Matrigel plugs were removed, photographed, viewed whole-mount by confocal microscopy (Nikon C1si), and then fixed and stained for fluorescence microscopy or homogenized, and the fluorescence content was quantified with a fluorimeter by using standard fluorescein filters (Tecan).

Pancreatic Carcinoma Model. The orthotopic pancreatic carcinoma model has been described (28, 29). Briefly, 6- to 10-week-old Tie2-GFP mice (30) were injected with 1 million syngeneic murine R40P cells in the tail of the pancreas. NPs containing Dox were injected i.v. on days 5, 7, and 9 postsurgical implantation of the cells. On day 11, the primary tumor and the hepatic hilar lymph node were resected and weighed. To quantify metastasis, the combined weight of both the lymph node and metastatic lesions is reported. Standard immunohistochemistry on frozen sections was performed. Images were acquired by using either a standard light microscope equipped with a CCD camera or confocal microscopy. The β3 integrin antibody was from BD Biosciences (550541). Blood vessels were labeled for ''EC markers'' with a mix of rat anti-mouse antibodies recognizing Flk-1 (BD Biosciences; 550549), CD31 (BD Biosciences; 550274), VE-cadherin (BD Biosciences; 555289), and CD105 (Millipore; CBL1358). The Apoptag kit from Millipore (S7165) was used as directed to assess apoptosis on frozen tissue sections. For targeting studies and biodistribution, fluorescent NPs (as described above) were injected on day 11, and the organs were resected at 5-h postinjection. The organs were imaged via whole mount on glass slides by confocal microscopy (Nikon C1si). Fluorescence was observed from both the NP and the blood vessels of the Tie2-GFP mice in which GFP was expressed in the endothelium.

Renal Cell Carcinoma Model. The renal cell carcinoma model was used as described (31). One million tumor cells in 20 μl of a 1:1 PBS/Matrigel mixture were injected into the lower pole of the kidney just below the renal subcapsule in male nu/nu mice. The needle was removed after a visible blister formed and leakage of the tumor cell suspension was minimal. Animals that formed visible blisters upon injection in the subcapsule with minimal leakage were used for the study. Mice with orthotopic injections of the SN12C-RFP cells were imaged by using the Olympus OV100 Small Animal Imaging System and grouped on day 7 based on weight and imaging results. NPs were injected i.v. every other day beginning on day 8 and continuing until the end of the

experiment when the kidneys were resected and weighed. The difference in weight between the tumor-bearing kidney and the normal kidney was reported. To observe metastasis, various organs, including the spleen, pancreas, diaphragm, lungs, liver, and intestines, were removed, and the RFP expression was imaged by using the OV100 system. Metastatic disease was quantified by measuring the total pixels in each organ with ImageJ software and quantifying the number of pixels in each image above a threshold of fluorescence intensity.

Statistical Analysis. Error bars represent mean values ± SEM. The statistical significance of the experiments was determined by two-tailed Student's *t* test. $P < 0.05$ were considered significant.

ACKNOWLEDGMENTS. This work was supported by National Cancer Institute Grant U54-CA119335 (National Cancer Institute Alliance for Nanotechnology in Cancer) (to D.A.C.) and National Institutes of Health Grants P01-CA078045 and P01-CA104898 (to D.A.C.).

1. Wang X, Huang DY, Huong SM, Huang ES (2005) Integrin αvβ3 is a coreceptor for human cytomegalovirus. *Nat Med* 11:515–521.
2. Wickham TJ, Mathias P, Cheresh DA, Nemerow GR (1993) Integrins αvβ3 and αvβ5 promote adenovirus internalization but not virus attachment. *Cell* 73:309–319.
3. Brooks PC, *et al.* (1994) Integrin αvβ3 antagonists promote tumor regression by inducing apoptosis of angiogenic blood vessels. *Cell* 79:1157–1164.
4. Brooks PC, *et al.* (1995) Antiintegrin αvβ3 blocks human breast cancer growth and angiogenesis in human skin. *J Clin Invest* 96:1815–1822.
5. Sipkins DA, *et al.* (1998) Detection of tumor angiogenesis *in vivo* by αvβ3-targeted magnetic resonance imaging. *Nat Med* 4:623–626.
6. Winter PM, *et al.* (2003) Molecular imaging of angiogenesis in nascent Vx-2 rabbit tumors using a novel αvβ3-targeted nanoparticle and 1.5 tesla magnetic resonance imaging. *Cancer Res* 63:5838–5843.
7. Arap W, Pasqualini R, Ruoslahti E (1998) Cancer treatment by targeted drug delivery to tumor vasculature in a mouse model. *Science* 279:377–380.
8. Hood JD, *et al.* (2002) Tumor regression by targeted gene delivery to the neovasculature. *Science* 296:2404–2407.
9. Gasparini G, *et al.* (1998) Vascular integrin αvβ3: A new prognostic indicator in breast cancer. *Clin Cancer Res* 4:2625–2634.
10. Weis SM (2007) Evaluating integrin function in models of angiogenesis and vascular permeability. *Methods Enzymol* 426:505–528.
11. Haubner R, *et al.* (1996) Structural and functional aspects of RGD-containing cyclic pentapeptides as highly potent and selective integrin αvβ3 antagonists. *J Am Chem Soc* 118:7461–7472.
12. Pfaff M, *et al.* (1994) Selective recognition of cyclic RGD peptides of NMR defined conformation by αIIbβ3, αvβ3, and α5β1 integrins. *J Biol Chem* 269:20233–20238.
13. Aguirre AJ, *et al.* (2003) Activated Kras and Ink4a/Arf deficiency cooperate to produce metastatic pancreatic ductal adenocarcinoma. *Genes Dev* 17:3112–3126.
14. House MG, *et al.* (2007) Prognostic significance of pathologic nodal status in patients with resected pancreatic cancer. *J Gastrointest Surg* 11:1549–1555.
15. Schwarz RE, Smith DD (2006) Extent of lymph node retrieval and pancreatic cancer survival: Information from a large U.S. population database. *Ann Surg Oncol* 13:1189–1200.
16. Allen TM, Cullis PR (2004) Drug delivery systems: Entering the mainstream. *Science* 303:1818–1822.
17. Hu G, *et al.* (2007) Imaging of Vx-2 rabbit tumors with αvβ-integrin-targeted 111In nanoparticles. *Int J Cancer* 120:1951–1957.
18. Pastorino F, *et al.* (2003) Vascular damage and antiangiogenic effects of tumor vessel-targeted liposomal chemotherapy. *Cancer Res* 63:7400–7409.
19. Schiffelers RM, *et al.* (2003) Antitumor efficacy of tumor vasculature-targeted liposomal doxorubicin. *J Controlled Release* 91:115–122.
20. Temming K, Schiffelers RM, Molema G, Kok RJ (2005) RGD-based strategies for selective delivery of therapeutics and imaging agents to the tumor vasculature. *Drug Resist Updat* 8:381–402.
21. Stewart PL, Nemerow GR (2007) Cell integrins: Commonly used receptors for diverse viral pathogens. *Trends Microbiol* 15:500–507.
22. Montet X, Funovics M, Montet-Abou K, Weissleder R, Josephson L (2006) Multivalent effects of RGD peptides obtained by nanoparticle display. *J Med Chem* 49:6087–6093.
23. Garanger E, Boturyn D, Coll JL, Favrot MC, Dumy P (2006) Multivalent RGD synthetic peptides as potent αvβ3 integrin ligands. *Org Biomol Chem* 4:1958–1965.
24. Takemura G, Fujiwara H (2007) Doxorubicin-induced cardiomyopathy from the cardiotoxic mechanisms to management. *Progr Cardiovas Dis* 49:330–352.
25. Steeghs N, Nortier JW, Gelderblom H (2007) Small molecule tyrosine kinase inhibitors in the treatment of solid tumors: An update of recent developments. *Ann Surg Oncol* 14:942–953.
26. Dai X, Su Z, Liu JO (2000) An improved synthesis of a selective αvβ3-integrin antagonist cyclo(-RGDfK-). *Tetrahedron Lett* 41:6295–6298.
27. Fritze A, Hens F, Kimpfler A, Schubert R, Peschka-Suss R (2006) Remote loading of doxorubicin into liposomes driven by a transmembrane phosphate gradient. *Biochim Biophys Acta* 1758:1633–1640.
28. Grimm J, Potthast A, Wunder A, Moore A (2003) Magnetic resonance imaging of the pancreas and pancreatic tumors in a mouse orthotopic model of human cancer. *Int J Cancer* 106:806–811.
29. Tsutsumi S, Yanagawa T, Shimura T, Kuwano H, Raz A (2004) Autocrine motility factor signaling enhances pancreatic cancer metastasis. *Clin Cancer Res* 10:7775–7784.
30. Motoike T, *et al.* (2000) Universal GFP reporter for the study of vascular development. *Genesis* 28:75–81.
31. An Z, Jiang P, Wang X, Moossa AR, Hoffman RM (1999) Development of a high metastatic orthotopic model of human renal cell carcinoma in nude mice: Benefits of fragment implantation compared to cell-suspension injection. *Clin Exp Metastasis* 17:265–270.